

~~CONFIDENTIAL~~ X 12 63918

Copy  
RM L56E25a

GPO PRICE \$

CFSTI PRICE(S) \$

\$2.00

Hard copy (HC)

Microfiche (MF) 1.50

First July 65

Declassified by authority of NASA  
Classification Change Notices No. 70  
Dated \*\* 4/20/64

# NACA

## RESEARCH MEMORANDUM

MINIMUM DRAG OF FOUR VERSIONS OF A SWEEP-WING  
FIGHTER AIRPLANE OBTAINED FROM FLIGHT  
TESTS OF ROCKET-BOOSTED MODELS AT  
MACH NUMBERS FROM 0.81 TO 1.71

By Earl C. Hastings, Jr.

Langley Aeronautical Laboratory  
Langlev Field, Va.

DECLASSIFIED- AUTHORITY  
US 1391 DROBKA TO LEBOW  
MEMO DATED 6/30/66

FACILITY FORM 602

N66 34100

(ACCESS OR NUMBER)

32

(PAGES)

(THRU)

1

(CODE)

02

(CATEGORY)

(NASA OR OR TMX OR AD NUMBER)

**NATIONAL ADVISORY COMMITTEE  
FOR AERONAUTICS**

WASHINGTON

September 7, 1956

## NATIONAL ADVISORY COMMITTEE FOR AERONAUTICS

## RESEARCH MEMORANDUM

MINIMUM DRAG OF FOUR VERSIONS OF A SWEEPED-WING  
FIGHTER AIRPLANE OBTAINED FROM FLIGHT  
TESTS OF ROCKET-BOOSTED MODELS AT  
MACH NUMBERS FROM 0.81 TO 1.71

By Earl C. Hastings, Jr.

## SUMMARY

Tests conducted with four specific versions of a swept-wing fighter airplane indicate that a large reduction in external-drag coefficient was accomplished by redesigning the original configuration.

The forebody modifications, which consisted of a smaller canopy, slimmer nose, and sharper inlet lip, reduced the value of the external-drag coefficient from 0.044 to 0.042 at a Mach number of 1.05 and from 0.042 to 0.040 at a Mach number of 1.28. Recontouring this modified fuselage by increasing the cross-sectional area ahead of and behind the wing to obtain a more efficient area distribution at a Mach number of 1.2 resulted in an additional drag reduction throughout the Mach number range of the tests. Values of external-drag coefficient from these tests were constant at 0.035 between Mach numbers of 1.05 and 1.71. The drag-rise Mach number for each configuration was 0.93.

## INTRODUCTION

An investigation has been conducted by the Langley Pilotless Aircraft Research Division to determine the minimum drag of four specific versions of a swept-wing fighter airplane. The first phase of the investigation was to determine the drag difference between two configurations with different canopy and nose shapes. A further investigation was then made to determine the minimum drag of the configuration redesigned with an area-rule application for a Mach number of 1.2 (refs. 1 and 2).

All of these tests were conducted at the Pilotless Aircraft Research Station at Wallops Island, Va. with rocket-boosted models of the various configurations.

### SYMBOLS

A	cross-section area, sq in.
$a_l/g$	longitudinal-accelerometer reading
$a_n/g$	normal-accelerometer reading
$\bar{c}$	mean aerodynamic chord
$C_c$	chord-force coefficient, positive in rearward direction, $- \frac{a_l}{g} \frac{W}{qS}$
$C_D$	drag coefficient, Drag/qS
$C_N$	normal-force coefficient, positive toward top of model, $\frac{a_n}{g} \frac{W}{qS}$
g	acceleration due to gravity, 32.2 ft/sec <sup>2</sup>
$\gamma$	flight-path angle, deg
k	ratio of specific heats
l	length, in.
M	Mach number
$m/m_0$	ratio of mass flow through duct to mass flow through a stream tube of area equal to inlet-capture area under free-stream conditions
p	static pressure, lb/sq ft
q	dynamic pressure, lb/sq ft



r radius, in.  
S total wing area (excluding chord extensions), sq ft  
t time, sec  
V velocity, ft/sec  
W weight, lb  
x station measured from nose, in.


## Subscripts:

b model base  
c choking-cup base  
e duct exit  
i duct inlet (capture)  
o free stream  
ext external  
int internal  
tot total

## MODELS AND TESTS

Figure 1 presents a three-view drawing of the final configuration tested. Since the primary difference in the four configurations was in cross-sectional-area development, only the one three-view drawing is presented; however the normal-cross-sectional-area distributions of the four configurations are shown as figures 2 to 6. The dimensional and mass characteristics are presented in table I.

Configuration 1 was a model of the first design proposal of a full-scale airplane. Configuration 2 had a modified forebody - an attempt to reduce the supersonic drag level. The modifications consisted of a smaller canopy, a slimmer and slightly longer forebody with a sharper nose, and a sharper inlet lip. Both of these models had internal flow and were not instrumented. Photographs of configurations 1 and 2 are shown in figures 7 and 8.



Reference 1 indicates that the zero-lift drag-rise increments associated with wings near the speed of sound can, in some cases, be reduced by changing the axial distribution of the fuselage cross-sectional area. Configurations 3 and 4 of the tests reported herein were developed on this principle by increasing the fuselage cross-sectional area of configuration 2 in front of and behind the wing in an attempt to further reduce the drag at supersonic speeds. This redistribution of cross-sectional area was made on the ducted model without appreciably changing the maximum cross-sectional area (fig. 6). A method used to determine cross-sectional-area distributions for supersonic Mach numbers is discussed in reference 2.

Configuration 3 had no underslung scoop inlet or internal flow and configuration 4 was ducted. Both models 3 and 4 contained internal telemeter systems to obtain flight data. Photographs of these models are shown in figures 9 and 10.

All of the models with internal flow (configurations 1, 2, and 4) had very similar ducting and bases. A single duct ran through the fuselage from the underslung scoop inlet to a single exit at the base. In order to choke the duct at flight Mach numbers greater than 1.0, each of these models had a choking cup installed at the duct exit. A sketch of the choking cup and base is also shown in figure 1. A slotted total-pressure tube was installed in the duct of configuration 4 ahead of this choking cup in order to obtain data necessary to compute internal drag.

The telemetered models (models 3 and 4) were instrumented to measure normal and longitudinal accelerations and free-stream total pressure. Configuration 4 was also instrumented to obtain values of duct total pressure. These models had four static-pressure orifices located on the base which were manifolded together to give an average static-pressure reading over the base. These quantities were transmitted from the model in flight to a ground receiving station where they were recorded.

Configurations 1 and 2 were boosted to Mach numbers of about 1.3 by using single 6.25-inch Deacon rocket motors. The Mach number range for configurations 3 and 4 was increased to about 1.7 by adding an additional ABL Deacon rocket motor to the booster stage. A photograph of one of the model-booster combinations is shown in figure 11.

A rawinsonde released at the time of firing obtained measurements of free-stream temperature, static pressure, and winds aloft. The velocity of the models and their positions in space were determined by a CW Doppler radar set and an NACA modified tracking radar unit, respectively.

## ANALYSIS OF DATA

The CW Doppler radar set was used to determine the total drag of all of the models during the decelerating portion of the flight. The method of analysis consists of differentiating the measured velocity with respect to time after correcting for flight-path angle and winds aloft. The total drag coefficient  $C_{D_{tot}}$  is reduced from the following equation:


$$C_{D_{tot}} = -\left(\frac{dV}{dt} + g \sin \gamma\right) \frac{W}{qSg}$$

Reference 3 discusses the operation of the CW Doppler radar set and the method of data analysis in more detail.

In addition to this method of determining drag, configurations 3 and 4 were instrumented so that normal-force and chord-force coefficients  $C_N$  and  $C_c$  could be computed. A comparison between chord-force coefficients determined from the rocket model of configuration 3 and unpublished wind-tunnel values of minimum-drag coefficient obtained for the same configuration (obtained in the Langley 8-foot transonic tunnel) showed agreement within the accuracy of the rocket-model tests. Therefore, the chord-force coefficients of the rocket models were assumed to represent the minimum-drag coefficients of the configurations.

In order to calculate the external-drag coefficient ( $C_{D_{ext}} = C_{D_{tot}} - C_{D_{int}} - C_{D_{base}}$ ) it was first necessary to compute the base and internal-drag coefficients. On the telemetered models the data necessary to calculate  $C_{D_{int}}$  and  $C_{D_{base}}$  were measured. Since the internal ducting and base arrangements of configurations 1 and 2 were so similar to those of configuration 4, values of  $C_{D_{int}}$  and  $C_{D_{base}}$  obtained from that test were assumed to apply for configurations 1 and 2 also.

As mentioned previously, each of the ducted models had a choking cup installed at the duct exit (fig. 1). Therefore the total base drag of these models was the sum of the base drag of the choking cups and the base drag of the models themselves. In the tests of configurations 3 and 4, the static pressure over the base of the models was measured. Because of the limited number of telemeter channels available however, the base static pressure of the choking cup was not measured in this test. Reference 4 presents data from a test where the base static pressure of a similar choking cup was obtained. These values of choking-cup



base pressure coefficient were assumed to apply to configurations 1, 2, and 4 of this investigation because of the similarity of the choking cup to the ones used herein. The total base-drag coefficient of configuration 4 was then computed as

$$C_{D_{base}} = \left[ \frac{-(p_b - p_o)(\text{Model base area})}{qS} \right] + \left[ \frac{-(p_c - p_o)(\text{Choking-cup base area})}{qS} \right]$$

Since configuration 3 had no choking cup,  $C_{D_{base}}$  for this configuration was determined from the first term in the above equation.

With the instrumented model of configuration 4 it was also possible to calculate the internal-drag coefficient by the method of reference 5. This method consists essentially of determining the loss in total momentum of air flowing through the duct between free stream and exit. The equation used for computing  $C_{D_{int}}$  is as follows:

$$C_{D_{int}} = \frac{2A_e}{S} \left[ \frac{m}{m_o} \left( \frac{A_1}{A_e} \right) - \frac{p_e}{p_o} \left( \frac{M_e}{M_o} \right)^2 - \left( \frac{p_e - p_o}{p_o k M_o^2} \right) \right]$$

This coefficient could only be determined in this test for Mach numbers greater than 1.0, since at lower Mach numbers the duct was unchoked and all of the data needed to satisfy the above equation could not be obtained.

#### QUALITY OF DATA

The quality of the Mach number and drag data presented in this paper is best illustrated by a comparison of the two sources of data collected from the tests of configurations 3 and 4. Both telemeter and tracking radar values of Mach number and total drag coefficient were available from these tests. The differences in these quantities as obtained by the two methods are presented at several Mach numbers in the following table:

	Configuration 3		Configuration 4	
	M = 1.03	M = 1.57	M = 1.10	M = 1.58
$\Delta$ Mach number	0.015	0.010	0.010	0.010
$\Delta C_{D_{tot}}$	0.0010	0.0015	0.0015	0.0015

Although no comparative data are available for models 1 and 2 because both Mach number and total drag coefficient were determined only from the tracking radar, it is believed that the quality of these data is as good as that for configurations 3 and 4.

When fairing curves through values of  $C_{D_{tot}}$  from the two sources of data from configurations 3 and 4, values obtained from the accelerometer data were weighted more heavily since they were believed to be the more reliable data from these tests.

Because of the similarity of the internal ducting and bases of the models with internal flow, the values of  $C_{D_{base}}$  and  $C_{D_{int}}$  obtained from the test of instrumented configuration 4 were assumed to apply to configurations 1 and 2 also. Even if a fairly large percentage of error in these values did exist between the configurations at supersonic speeds, this difference would have a negligible effect on the overall external-drag coefficients since the magnitude of the errors would be quite small.

#### TEST CONDITIONS

The conditions for the four-rocket-model drag tests in terms of Reynolds number, trim normal-force coefficient, and mass-flow ratio are presented in figures 12, 13, and 14, respectively.

Reynolds number values (based on the length of the mean aerodynamic chord) are plotted against Mach number for each configuration in figure 12. Values for configurations 1 and 2 are consistently larger at comparable Mach numbers than those for configurations 3 and 4. This is primarily due to the lower altitudes at which tests of configurations 1 and 2 were conducted.

Trim normal-force coefficient  $C_{N_{trim}}$  is presented for the instrumented configurations 3 and 4 in figure 13. These models were flown with center-of-gravity locations of 6.95 and 6.56 percent of the mean aerodynamic chord, respectively. Agreement between the two curves is good. The transonic trim change is small, amounting to about 0.050 between  $M = 0.93$  and  $0.99$ . Since configurations 1 and 2 were both tested with center-of-gravity locations of 7.0 percent of the mean aerodynamic chord and were quite similar geometrically to configurations 3 and 4, values of  $C_{N_{trim}}$  for configurations 1 and 2 are believed to be essentially the same as those shown for 3 and 4 in figure 13.

The mass-flow ratio  $m/m_0$  of ducted configuration 4 is presented in figure 14. Above  $M = 1.01$  the values shown were computed from



measured data. At Mach numbers less than 1.0 it was possible to estimate  $m/m_0$  by assuming that the static pressure at the duct exit was the same as that measured on the base of the model. This estimated curve is also shown in figure 14 along with estimated values of  $m/m_0$  for configurations 1 and 2 computed at  $M = 1.0$ .


## RESULTS AND DISCUSSION

Figure 15 presents the total drag coefficient for configurations 1, 2, 3, and 4. These values include the base drag of each model and the internal drag of the ducted models. Data presented for configurations 1 and 2 were obtained only from the CW Doppler radar unit, but values of  $C_{D_{tot}}$  from both telemeter data and tracking radar are shown for configurations 3 and 4. The agreement between the two sources of data for configurations 3 and 4 is considered very good throughout the supersonic Mach number range.

The internal-drag coefficient as determined from the test of configuration 4 is presented in figure 16. These values are small with a maximum  $C_{D_{int}}$  of 0.0010 occurring at  $M = 1.71$ . Between Mach numbers of 0.81 and 1.29,  $C_{D_{int}}$  is assumed to be zero. Also shown in figure 16 are values of  $C_{D_{base}}$  for configurations 3 and 4. Since configuration 3 was not ducted, the base geometry of this configuration differed considerably from that of the other three models. As mentioned previously, the values of  $C_{D_{base}}$  and  $C_{D_{int}}$  for configuration 4 are assumed to apply to the other ducted models.

Figure 17 presents  $C_{D_{ext}}$  for each of the four configurations. Configuration 2 with the smaller canopy and sharper nose and inlet lip had values of  $C_{D_{ext}}$  which were 0.002 lower than those of configuration 1 between Mach numbers of 1.05 and 1.28. These modifications resulted in a decrease in  $C_{D_{ext}}$  from 0.044 to 0.042 at  $M = 1.05$  and from 0.042 to 0.040 at  $M = 1.28$ . There was no change in the drag-rise Mach number which was 0.93 (based on  $dC_D/dM = 0.10$ ) in both cases. The subsonic-drag level in both cases was 0.017.

When the fuselage of configuration 2 was recontoured (based on an area-rule application at  $M = 1.2$ ), a large drag reduction was achieved throughout the supersonic range of the tests. Both configurations 3 and 4 show  $C_{D_{ext}} = 0.035$  between Mach numbers of 1.05 and approximately 1.7. Subsonic-drag levels of configurations 3 and 4 were 0.015



and 0.017, respectively. The drag-rise Mach numbers of both of these configurations were again 0.93.

The data presented in figure 17 show that the redesign of the nose and canopy reduces  $C_{D_{ext}}$  by about 5 percent at  $M = 1.28$ . By recontouring the fuselage with only small changes in the maximum cross-sectional area, an additional 12-percent decrease is realized at the same Mach number.

### CONCLUSIONS


Results of minimum-drag tests of four specific versions of a swept-wing fighter-type airplane indicate the following conclusions:

1. The configuration with the modified forebody (smaller canopy, sharper nose, and inlet lip) showed reduced values of external-drag coefficient at low supersonic Mach numbers. The modifications decreased the external-drag coefficient from 0.044 to 0.042 at a Mach number of 1.05 and from 0.042 to 0.040 at a Mach number of 1.28.

2. When the fuselage of the modified configuration was recontoured for an area-rule application at Mach number 1.2, the external-drag coefficient was further reduced to 0.035 between Mach numbers of 1.05 and 1.71.

3. The drag-rise Mach number for each configuration was 0.93.

Langley Aeronautical Laboratory,  
National Advisory Committee for Aeronautics,  
Langley Field, Va., May 11, 1956.





## REFERENCES

1. Whitcomb, Richard T.: A Study of the Zero-Lift Drag-Rise Characteristics of Wing-Body Combinations Near the Speed of Sound. NACA RM L52H08, 1952.
2. Holdaway, George H.: Comparison Of Theoretical and Experimental Zero-Lift Drag-Rise Characteristics Of Wing-Body-Tail Combinations Near the Speed Of Sound. NACA RM A53H17, 1953.
3. Wallskog, Harvey A., and Hart, Roger G.: Investigation of the Drag of Blunt-Nosed Bodies of Revolution in Free Flight at Mach Numbers From 0.6 to 2.3. NACA RM L53D14a, 1953.
4. Mitcham, Grady L., and Blanchard, Willard S., Jr.: Low-Lift Drag and Stability Data From Rocket Models of a Modified-Delta-Wing Airplane With and Without External Stores at Mach Numbers From 0.8 to 1.36. NACA RM L53A27, 1953.
5. Sears, R. I., and Merlet, C. F.: Flight Determination of the Drag and Pressure Recovery of an NACA 1-40-250 Nose Inlet at Mach Numbers From 0.9 to 1.8. NACA TN 3218, 1955. (Supersedes NACA RM L50L18.)



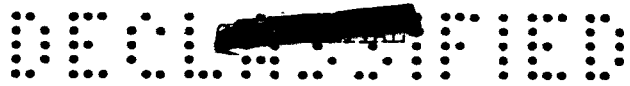


TABLE I

DIMENSIONAL AND MASS CHARACTERISTICS OF CONFIGURATIONS

Wing:

Total area (excluding chord extensions), sq ft . . . . .	4.53
Aspect ratio . . . . .	3.40
Mean aerodynamic chord (excluding chord extensions) . . . . .	1.29
Incidence angle, deg . . . . .	-1
Dihedral angle, deg . . . . .	-5
Sweepback (quarter-chord line), deg . . . . .	42
Airfoil section at root, parallel to free-stream direction . . . . .	NACA 65A006
Airfoil section at tip, parallel to free-stream direction . . . . .	NACA 65A005
Taper ratio . . . . .	0.25
Span, ft . . . . .	3.92

Vertical tail (extended to model center line and not including dorsal fin):

Area, sq ft . . . . .	1.19
Aspect ratio . . . . .	1.50
Sweepback (quarter-chord line), deg . . . . .	45
Taper ratio . . . . .	0.26
Span, ft . . . . .	1.33
Airfoil section at tip . . . . .	NACA 65A004
Airfoil section, 3.02 inches above fuselage center line . . . . .	NACA 65A006

	Configurations 1 and 2	Configurations 3 and 4
Horizontal tail:		
Total area, sq ft . . . . .	1.28	1.14
Aspect ratio . . . . .	3.5	3.5
Incidence angle, deg . . . . .	0	0
Dihedral angle, deg . . . . .	5.4	5.4
Sweepback (quarter-chord line), deg . . . . .	45	45
Airfoil section at root, parallel to free-stream direction . . . . .	NACA 65A006	NACA 65A006
Airfoil section at tip, parallel to free-stream direction . . . . .	NACA 65A004	NACA 65A004
Taper ratio . . . . .	0.15	0.15
Span, ft . . . . .	2.12	1.99



TABLE I.- Concluded  
 DIMENSIONAL AND MASS CHARACTERISTICS OF CONFIGURATIONS

	Configuration 1	Configuration 2	Configuration 3	Configuration 4
<b>Fuselage:</b>				
Maximum total frontal area, sq ft . . .	0.31	0.31	0.34	0.34
Length, ft . . . . .	5.58	5.62	6.08	5.80
Base area, sq ft . . . . .	0.07	0.07	0.11	0.06
Fuselage nose to wing leading edge at center line, ft . . . . .	1.97	2.00	2.36	2.08
Fuselage nose to horizontal-tail leading edge at center line, ft . . . . .	4.51	4.54	4.78	4.52
<b>Duct:</b>				
Inlet capture area, sq ft . . . . .	0.049	0.052	-----	0.051
Exit area, sq ft . . . . .	0.044	0.049	-----	0.043
Choking-cup base area, sq ft . . . . .	0.014	0.010	-----	0.014
<b>Weight and balance:</b>				
Weight, lb . . . . .	148.4	142.2	174.75	158.50
Wing loading, lb/sq ft . . . . .	32.8	31.5	38.6	35.0
Center-of-gravity location, percent $\bar{c}$ . . . . .	7.0	7.0	6.95	6.56

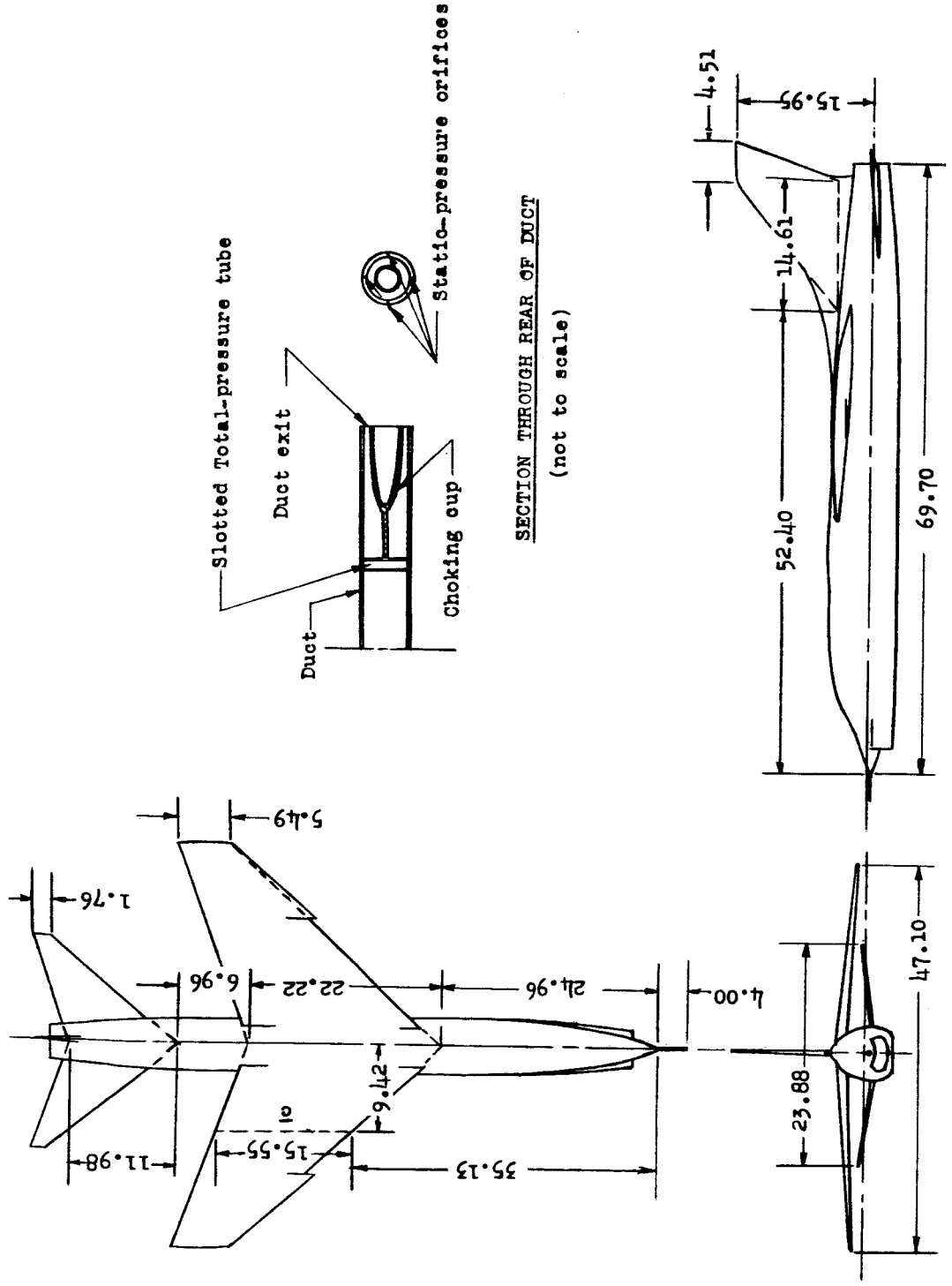
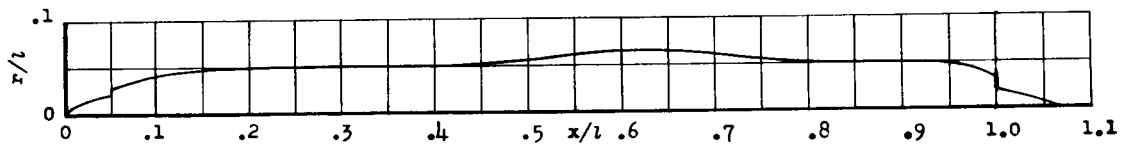
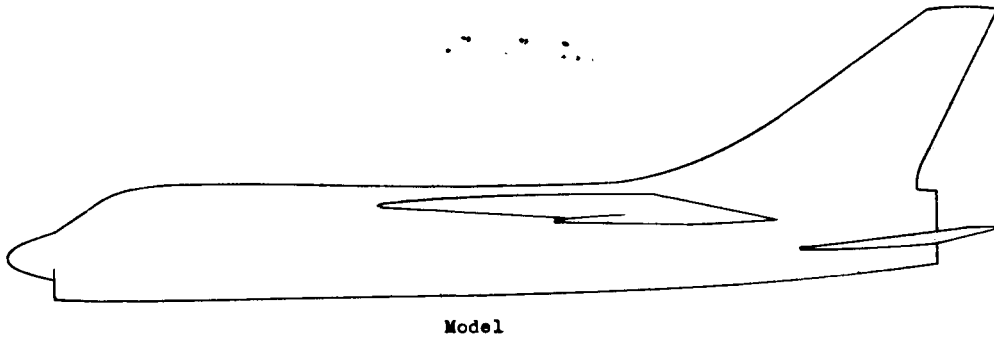
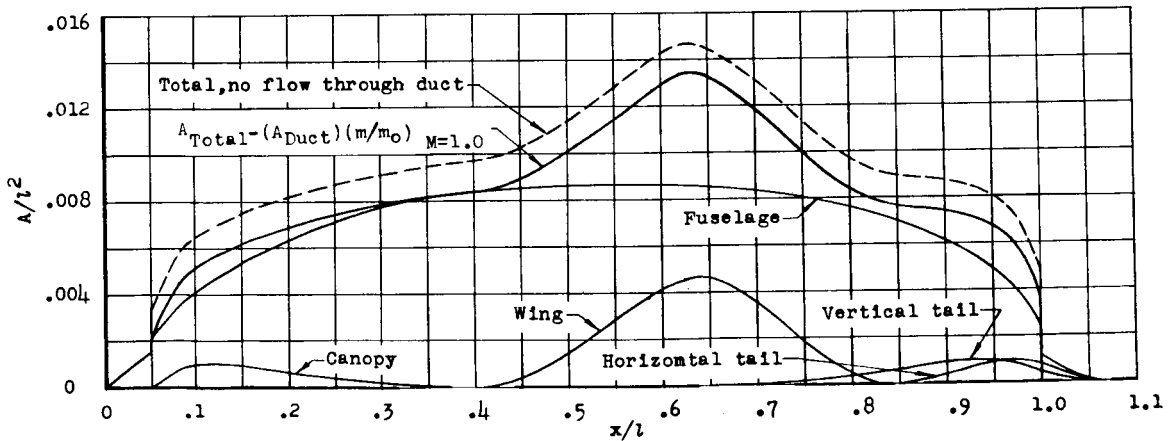


Figure 1.- Three-view drawing of configuration 4. (All dimensions are in inches.)





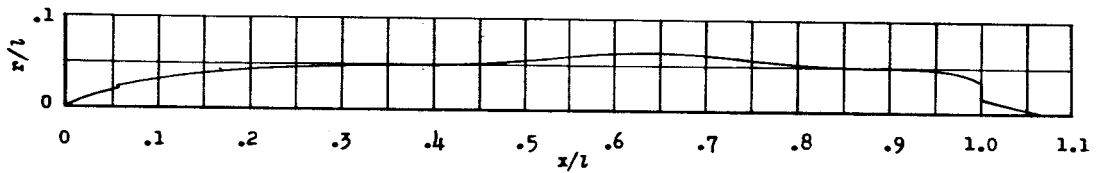
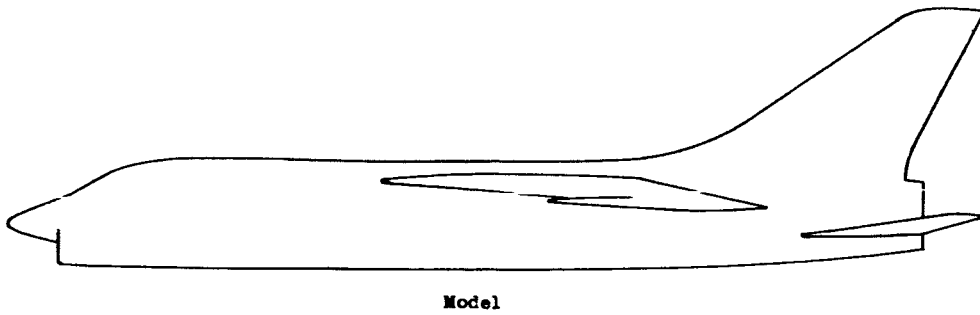
(a) Equivalent body (complete model).



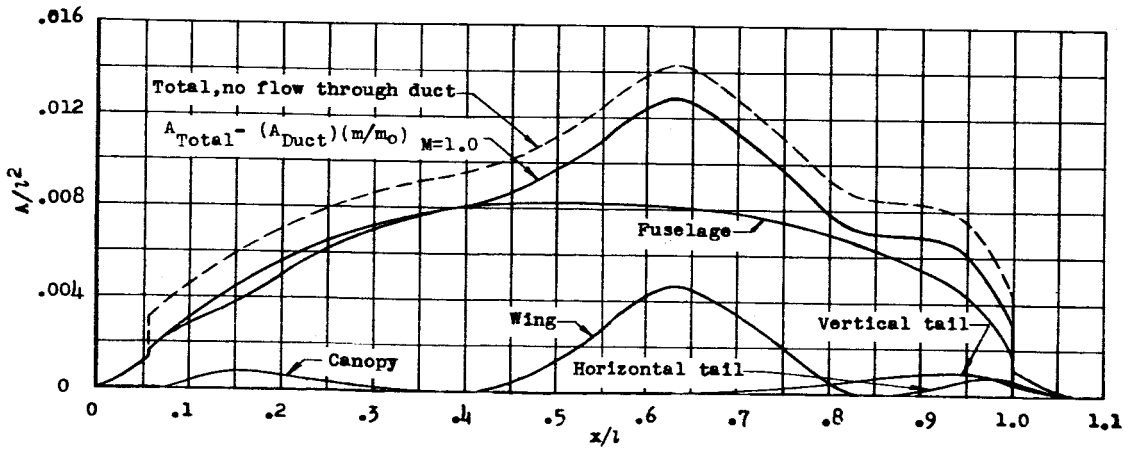
(b) Normal-cross-sectional-area distribution.

Figure 2.- Equivalent body and normal cross-sectional area of configuration 1.





(a) Equivalent body (complete model).

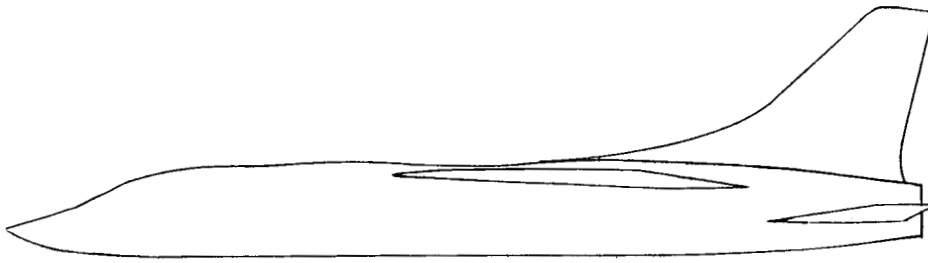


(b) Normal-cross-sectional-area distribution.

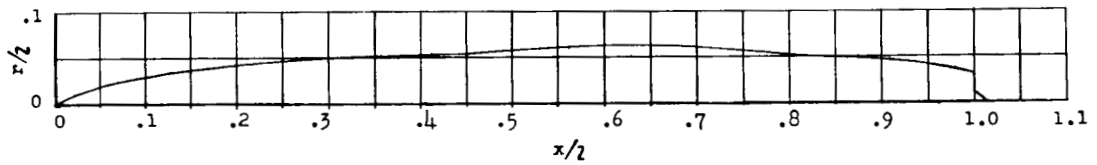
Figure 3.- Equivalent body and normal cross-sectional area of configuration 2.



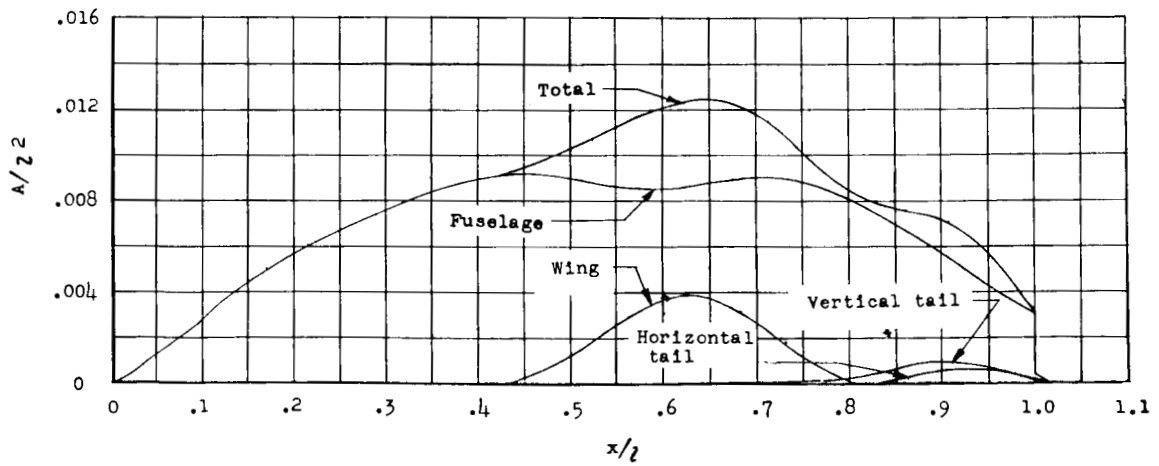




Model



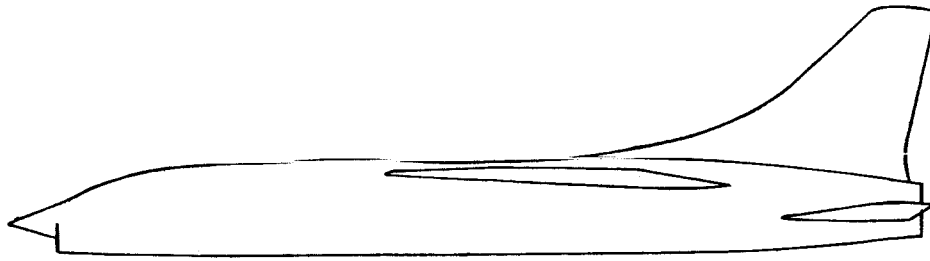
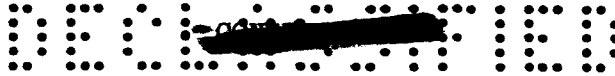
(a) Equivalent body (complete model).



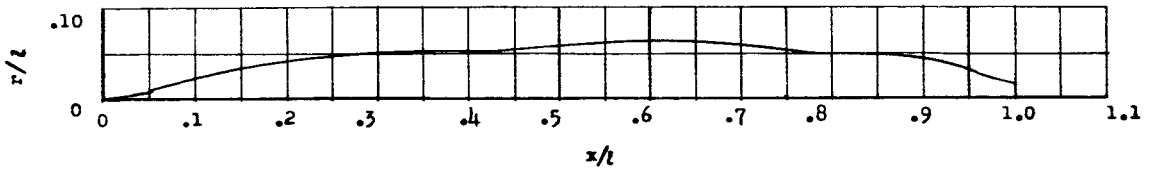
(b) Normal-cross-sectional-area distribution.

Figure 4.- Equivalent body and normal cross-sectional area of configuration 3.

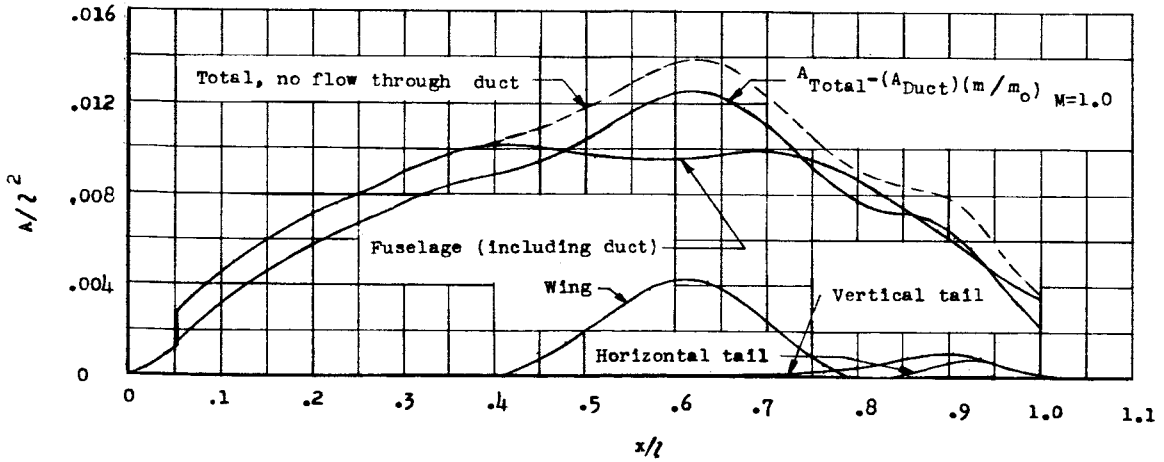




Model



(a) Equivalent body (complete model).



(b) Normal-cross-sectional-area distribution.

Figure 5.- Equivalent body and normal cross-sectional area of configuration 4.



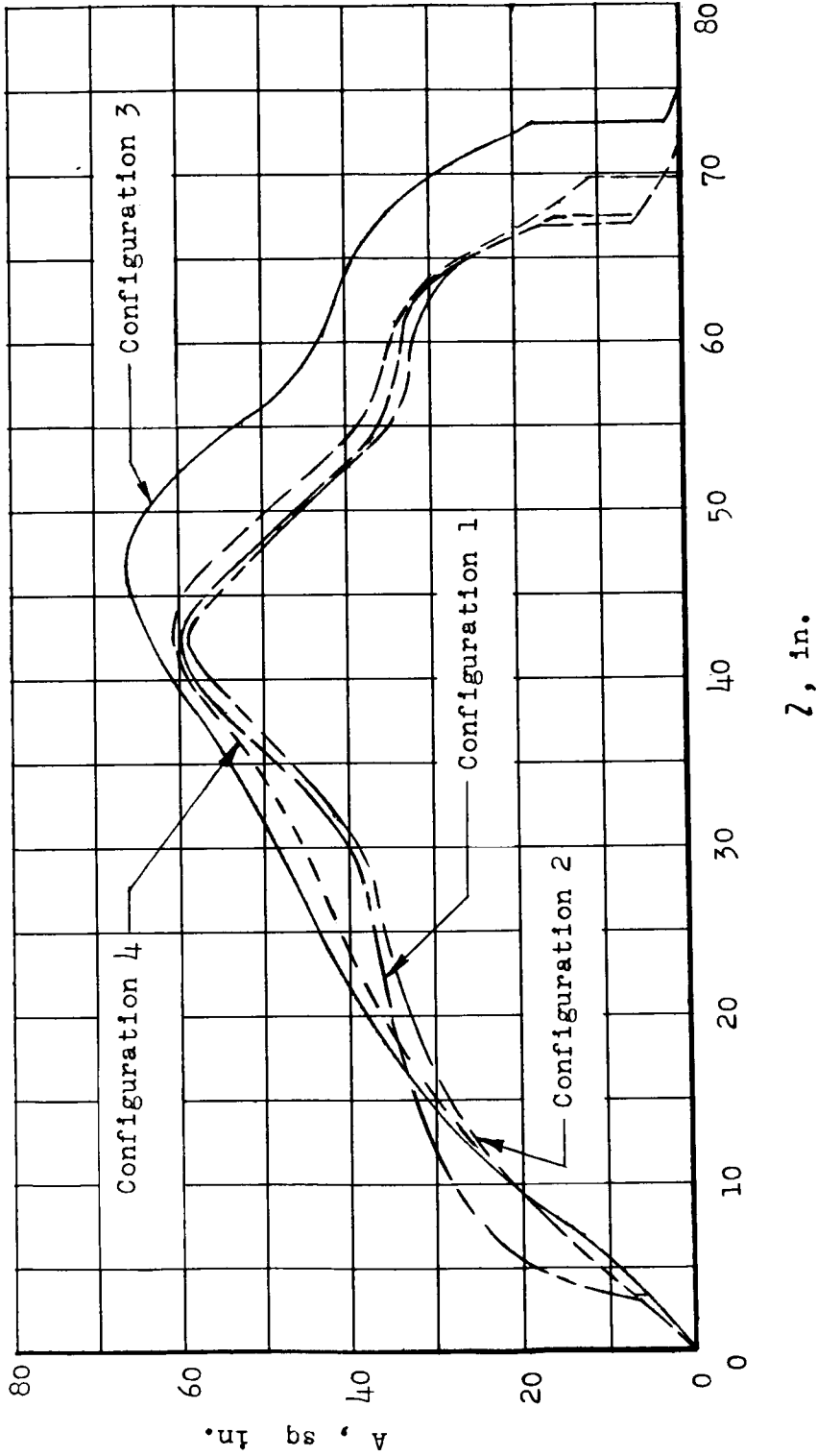
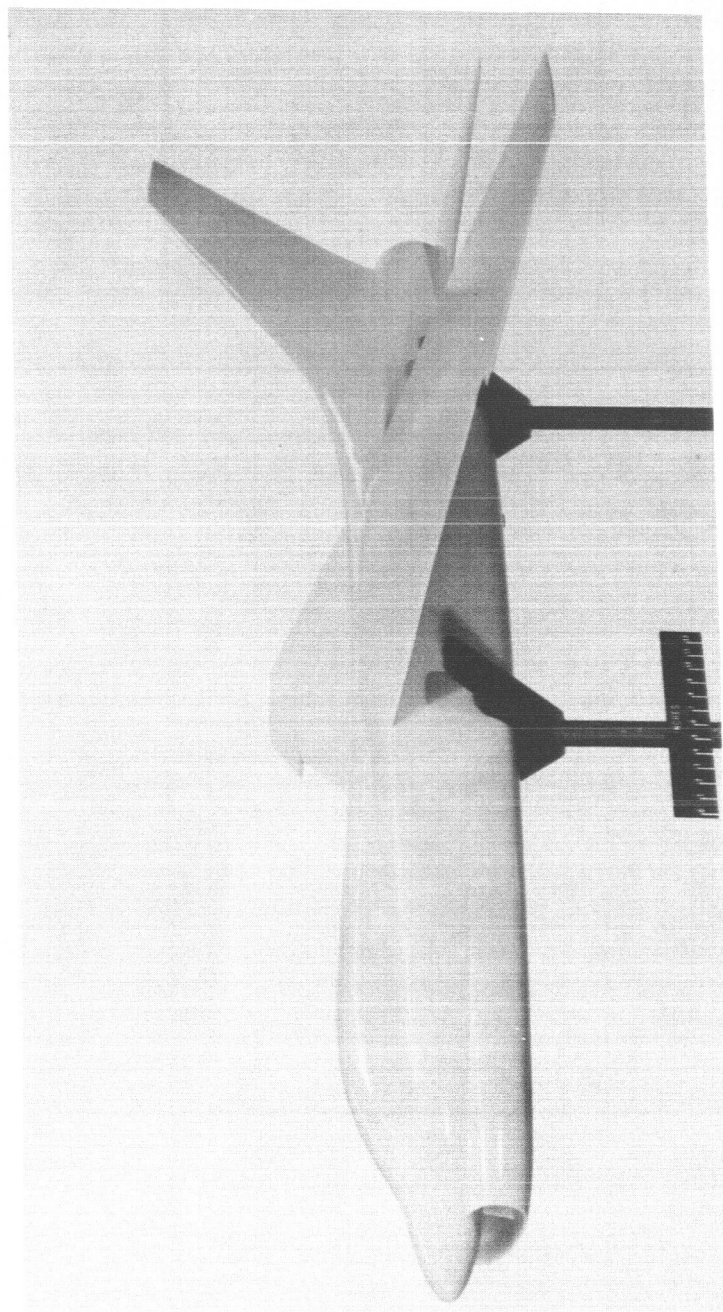
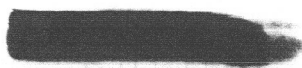


Figure 6.-- Normal cross-sectional area of configurations 1, 2, 3, and 4 (ducted configurations corrected for internal flow).

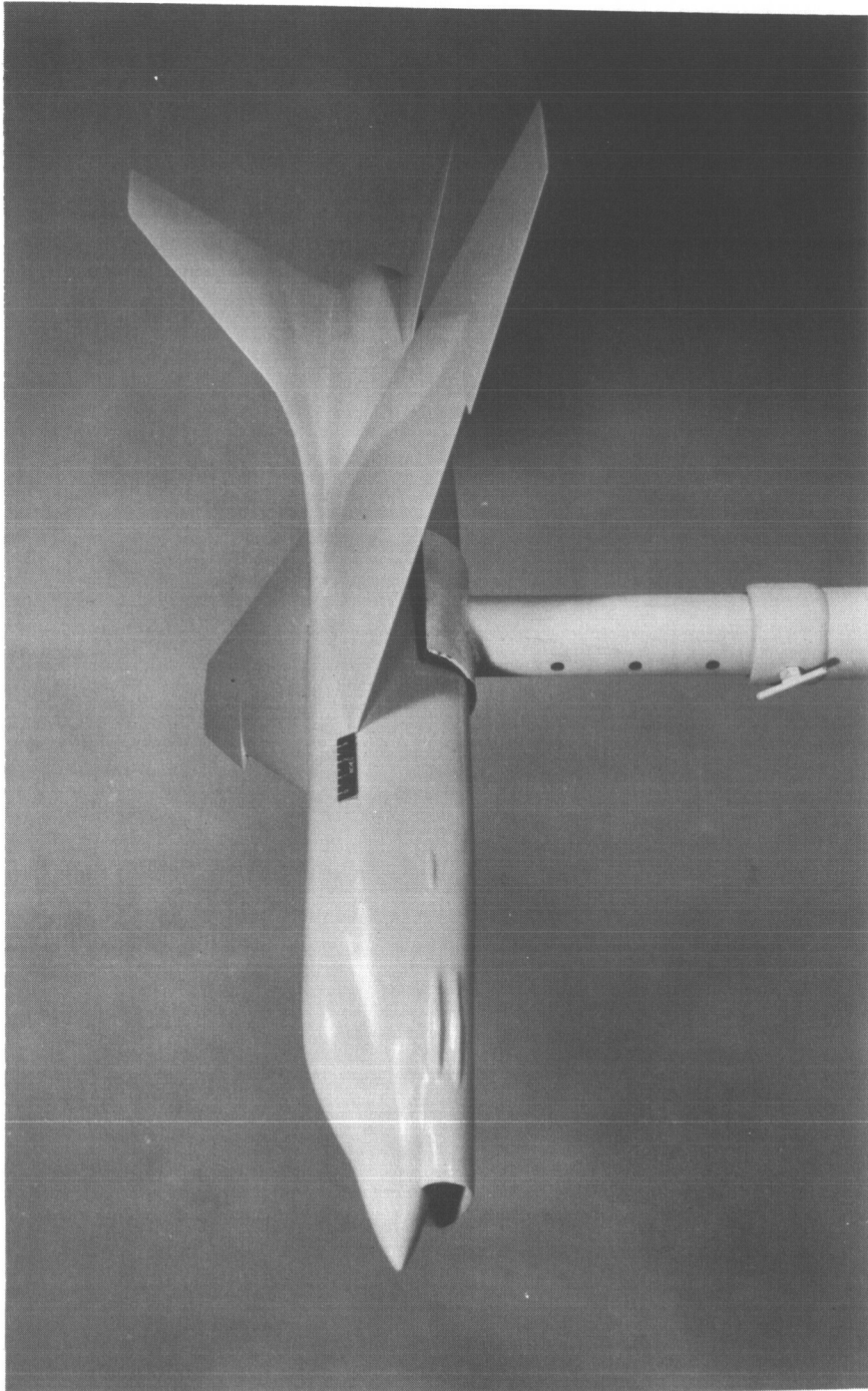


L-81834

Figure 7.- Configuration 1.



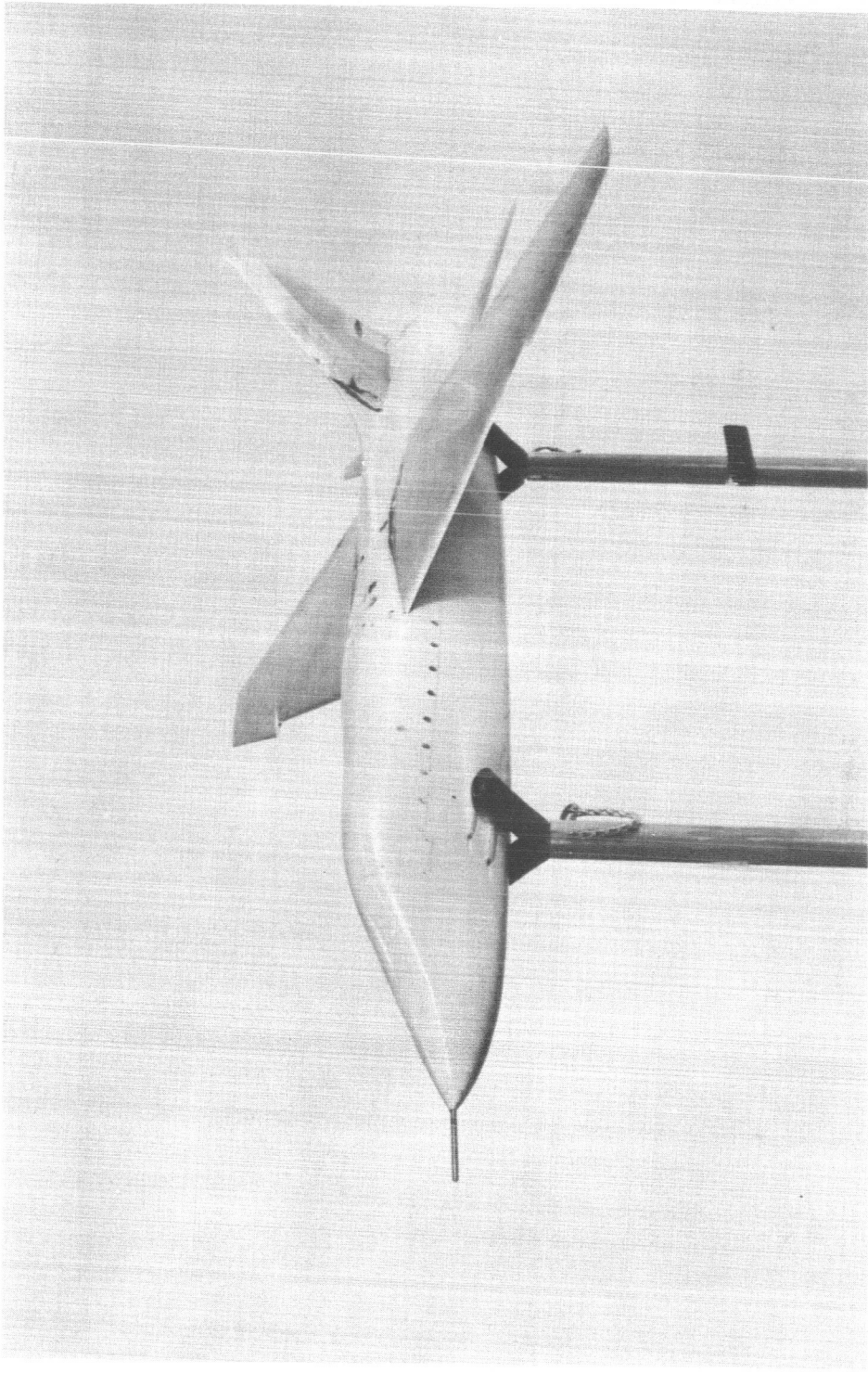
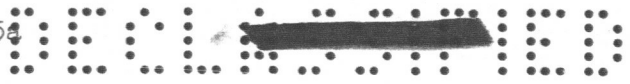
~~CONFIDENTIAL~~



L-82838

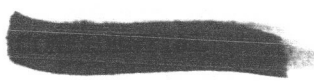
Figure 8.- Configuration 2.

~~CONFIDENTIAL~~

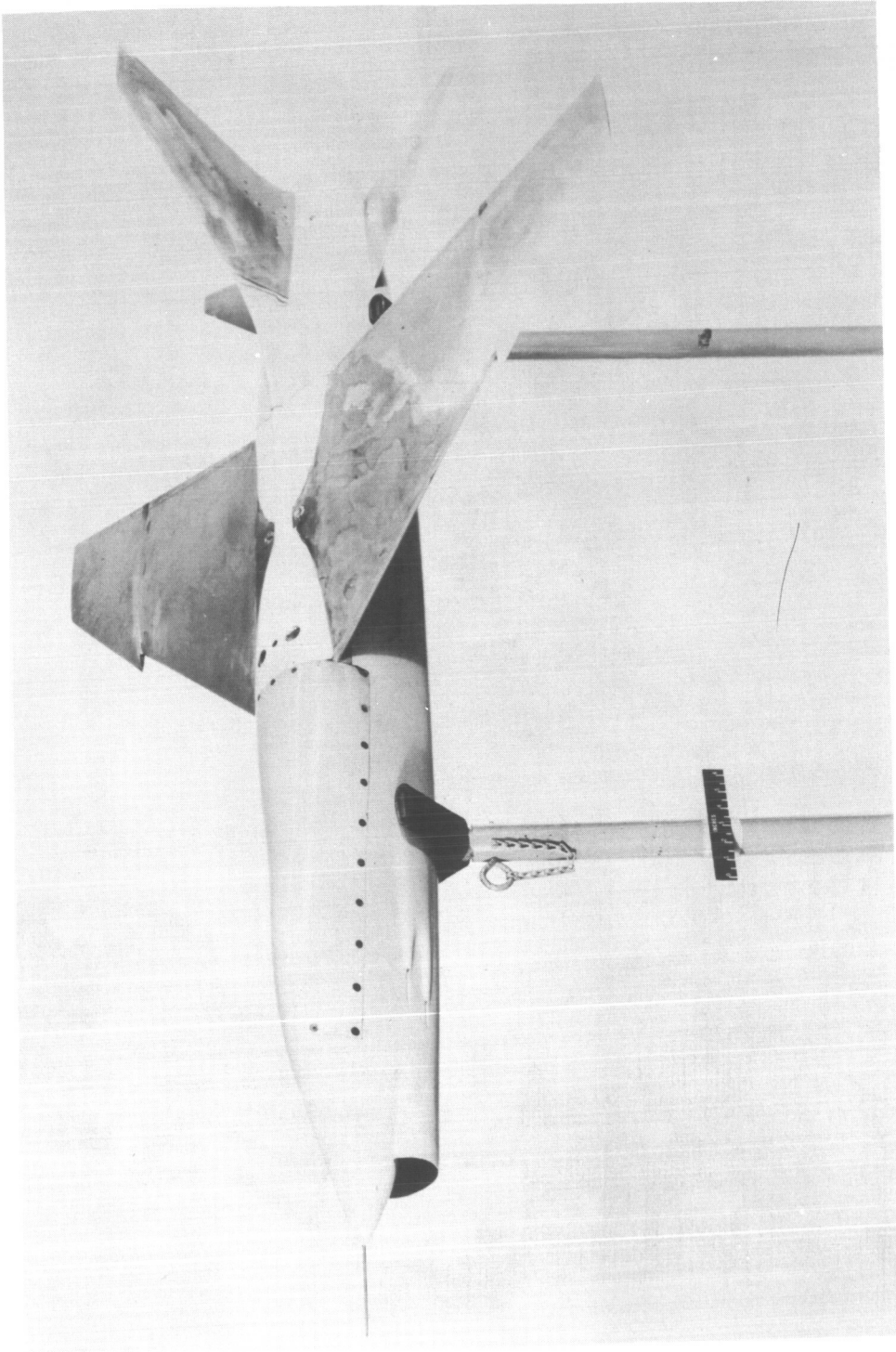


L-89402.1

Figure 9.- Configuration 3.



~~CONFIDENTIAL~~



L-90885.1

Figure 10.- Configuration 4.

~~CONFIDENTIAL~~



L-89540.1

Figure 11.- Model-booster combination prior to launching.





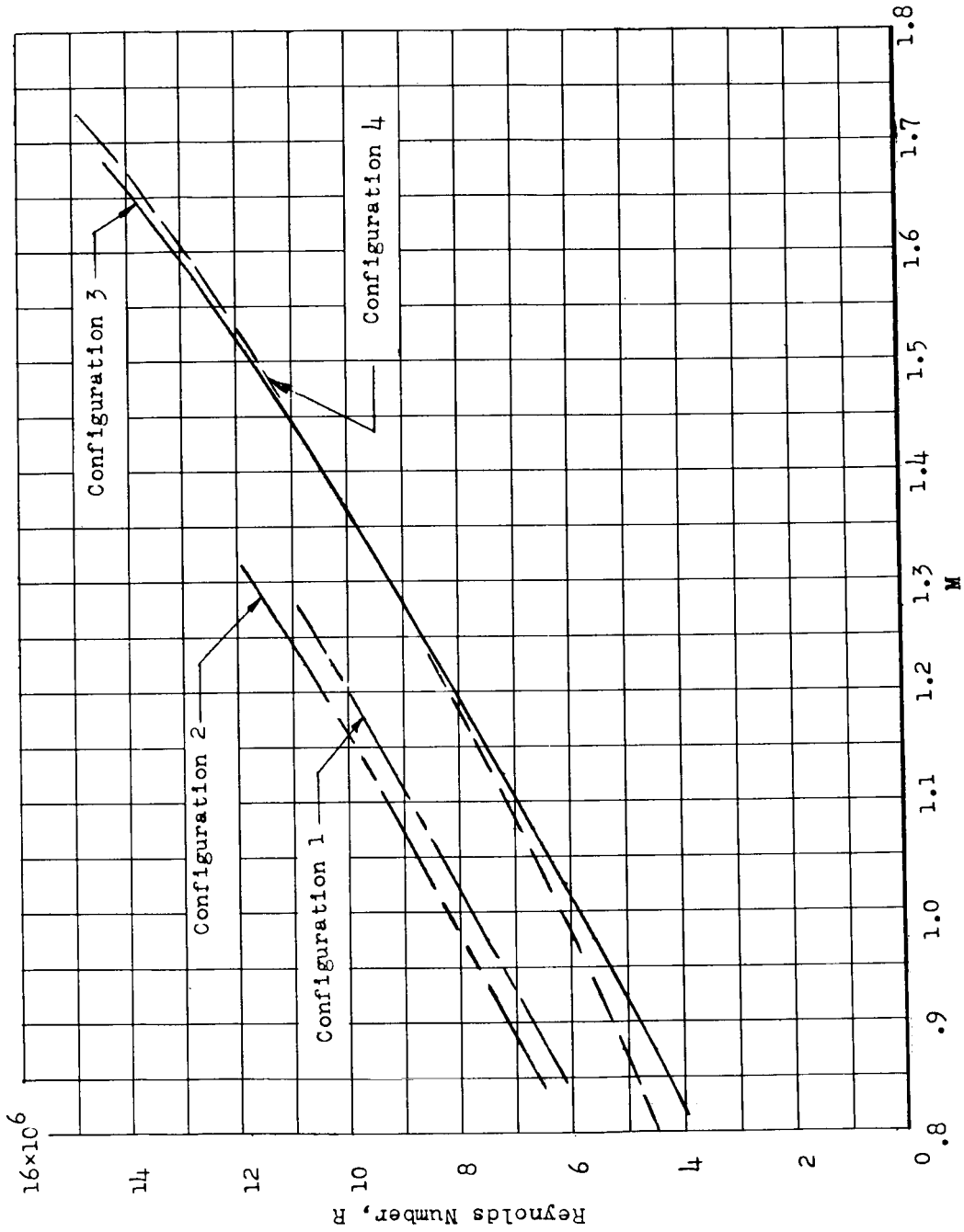


Figure 12.- Reynolds number (based on mean aerodynamic chord).

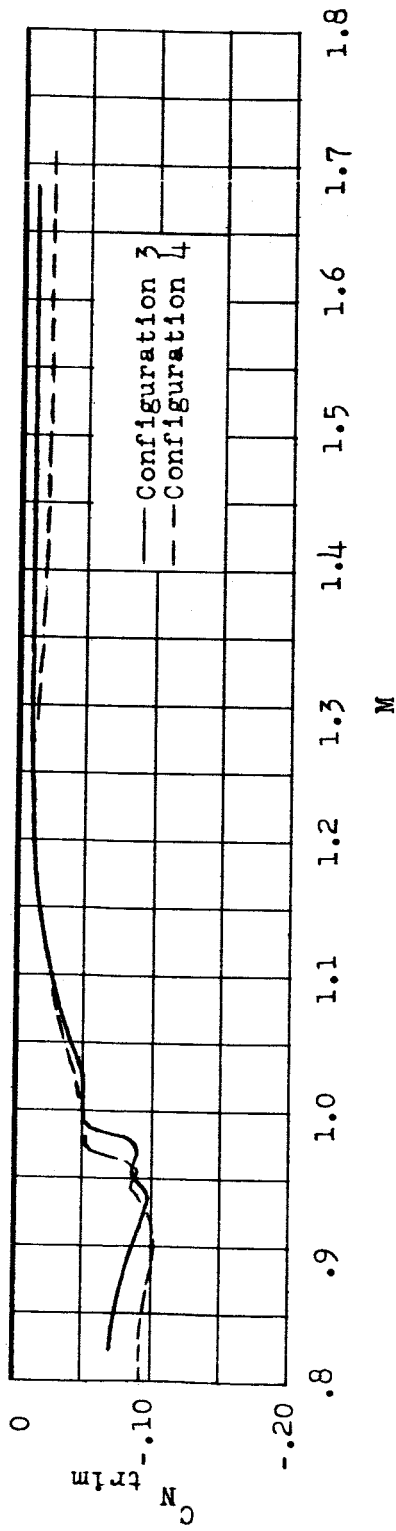


Figure 13.- Trim normal-force coefficient of configurations 3 and 4.

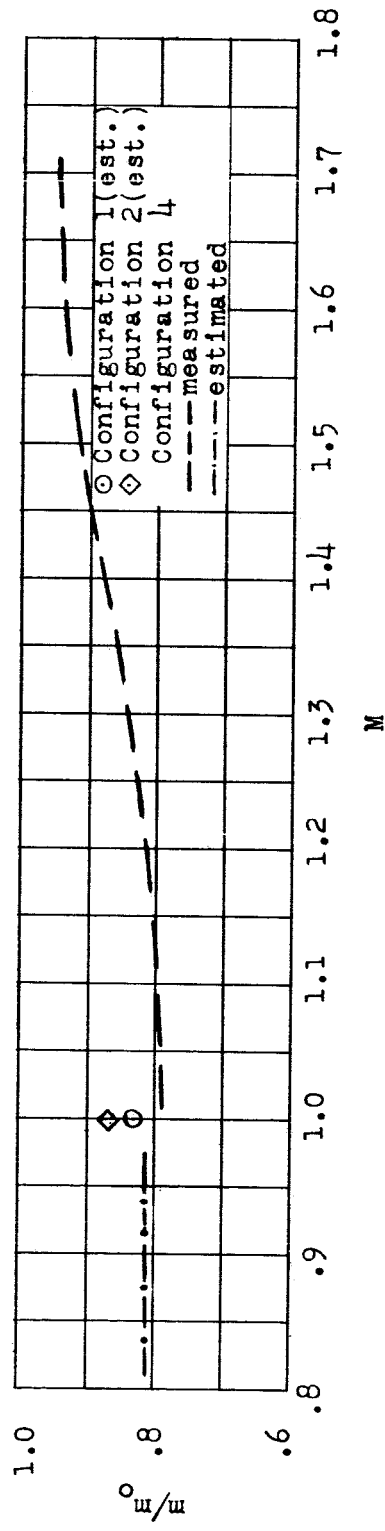


Figure 14.- Mass-flow ratio.



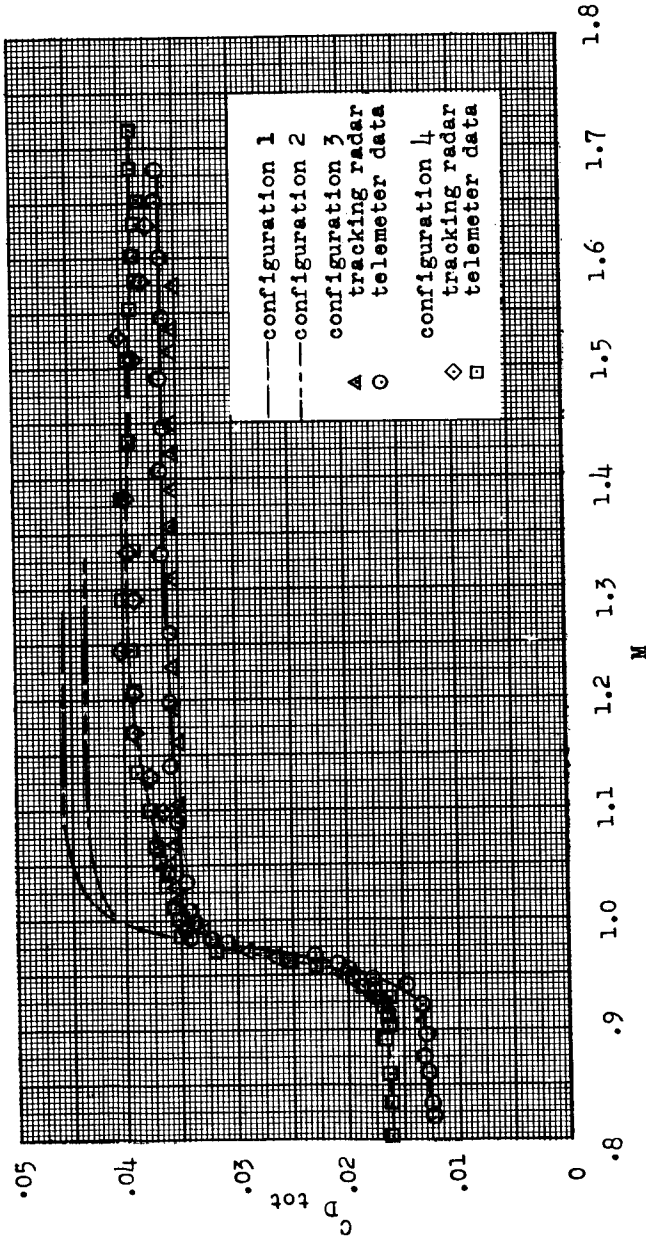


Figure 15.- Total drag coefficient.

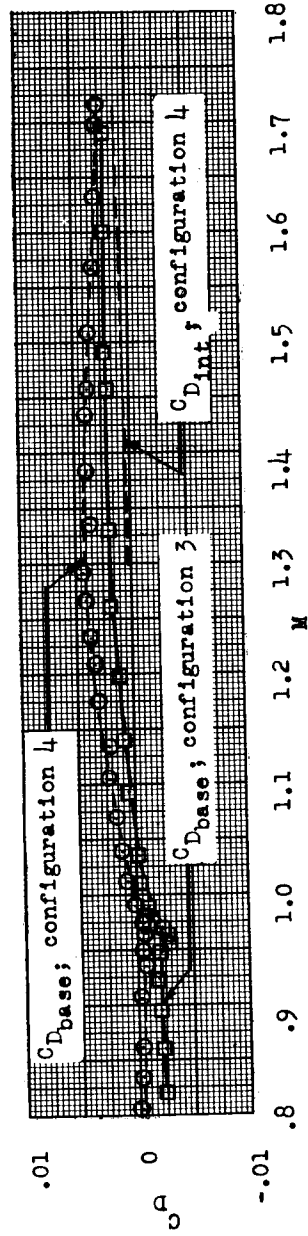


Figure 16.- Internal- and base-drag coefficients of configurations 3 and 4.

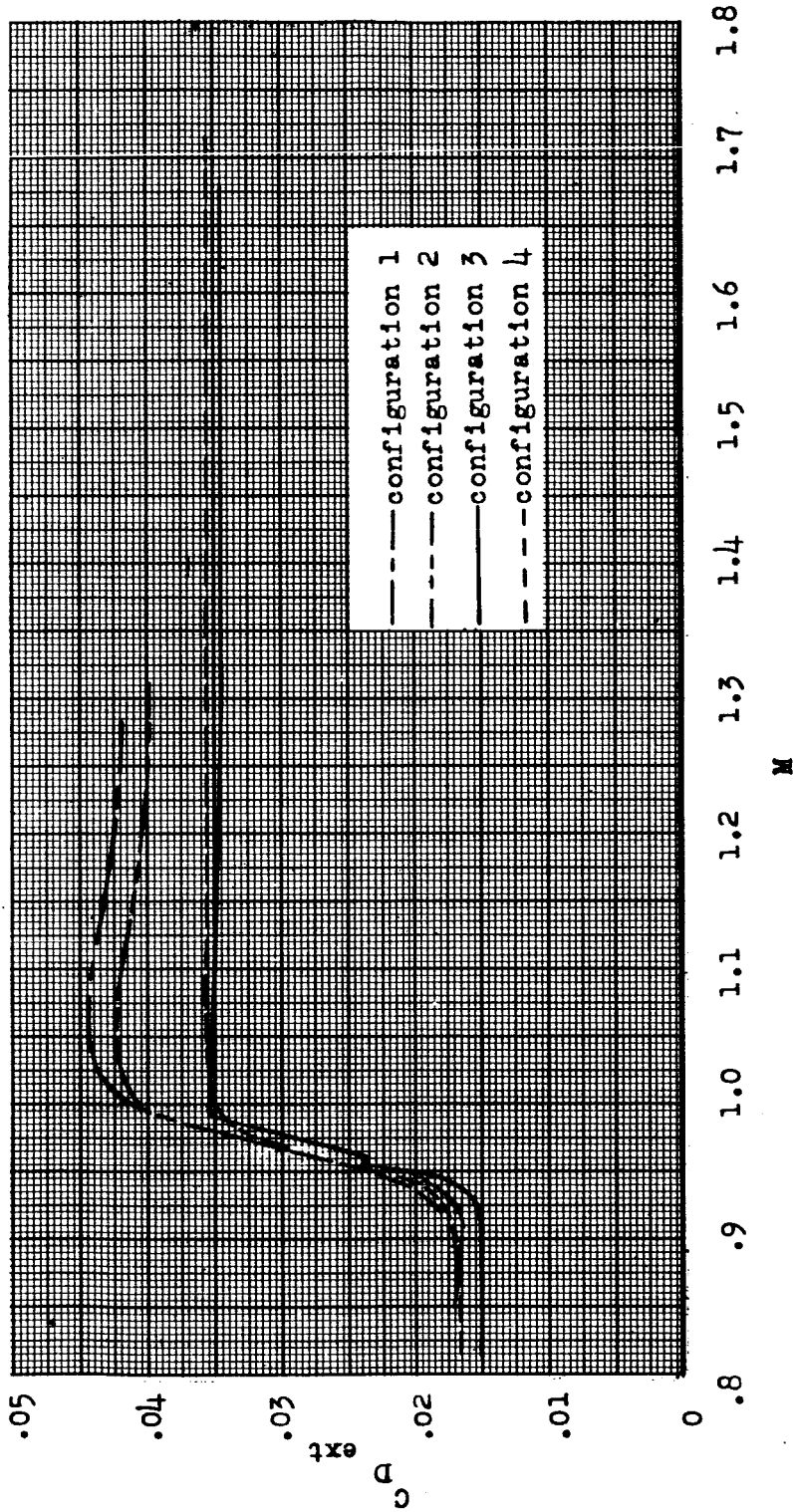
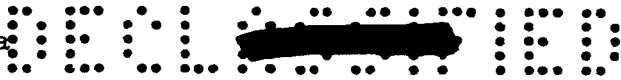


Figure 17.- External-drag coefficient.

